

# When Schrödinger Bridge Meets Real-World Image Dehazing with Unpaired Training

Yunwei Lan<sup>1,2</sup>, Zhigao Cui<sup>1\*</sup>, Xin Luo<sup>2</sup>, Chang Liu<sup>2</sup>, Nian Wang<sup>1</sup>,  
Menglin Zhang<sup>2</sup>, Yanzhao Su<sup>1</sup>, Dong Liu<sup>2\*</sup>

<sup>1</sup>Rocket Force University of Engineering, Xi'an 710025, China

<sup>2</sup>MOE Key Laboratory of Brain-Inspired Intelligent Perception and Cognition,  
University of Science and Technology of China, Hefei 230093, China

## Abstract

Recent advancements in unpaired dehazing, particularly those using GANs, show promising performance in processing real-world hazy images. However, these methods tend to face limitations due to the generator's limited transport mapping capability, which hinders the full exploitation of their effectiveness in unpaired training paradigms. To address these challenges, we propose *DehazeSB*, a novel unpaired dehazing framework based on the Schrödinger Bridge. By leveraging optimal transport (OT) theory, *DehazeSB* directly bridges the distributions between hazy and clear images. This enables optimal transport mappings from hazy to clear images in fewer steps, thereby generating high-quality results. To ensure the consistency of structural information and details in the restored images, we introduce detail-preserving regularization, which enforces pixel-level alignment between hazy inputs and dehazed outputs. Furthermore, we propose a novel prompt learning to leverage pre-trained CLIP models in distinguishing hazy images and clear ones, by learning a haze-aware vision-language alignment. Extensive experiments on multiple real-world datasets demonstrate our method's superiority. Code: <https://github.com/ywxjm/DehazeSB>.<sup>1</sup>

## 1. Introduction

Images captured under hazy conditions usually display reduced brightness and diminished contrast, significantly degrading visual quality and hindering further applications in visual tasks such as object detection [11]. Consequently, image dehazing, which aims to restore clear images from

<sup>1</sup>We acknowledge the support of GPU cluster built by MCC Lab of Information Science and Technology Institution, USTC. Corresponding authors: Zhigao Cui and Dong Liu. (ywl, xinluo, lc980413, zhangmenglin)@mail.ustc.edu.cn, cuizg10@126.com, nianwang04@outlook.com, syzlh@163.com, dongeliu@ustc.edu.cn

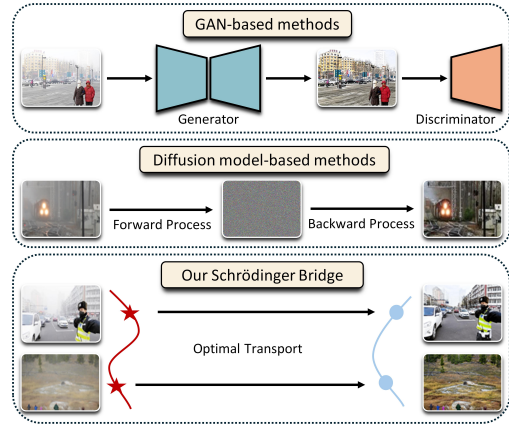


Figure 1. Existing GAN-based unpaired dehazing methods struggle to handle images with complex structures due to the limited mapping capability of the generator. While **diffusion model-based methods** can achieve more intricate transport mappings, they necessitate transforming images into Gaussian noise and then regenerating them through a large number of sampling steps. **Our Schrödinger Bridge** enables the direct learning of optimal transport mapping from hazy to clear image distributions in fewer time steps, achieving high efficiency and high-quality dehazing.

hazy ones, has received considerable attention over the past decade. The degradation process of hazy images typically adheres to the Atmospheric Scattering Model (ASM) [31].

$$I(x) = J(x)t(x) + A(1 - t(x)), \quad (1)$$

where  $I(x)$  represents the hazy image, and  $J(x)$  is the corresponding clear one.  $A$  and  $t(x)$  are the atmospheric light and transmission map.

Early studies [3, 16, 51] primarily rely on physical priors to estimate the parameters necessary for the ASM, subsequently obtaining clear images. Although these methods can effectively dehaze images, they are susceptible to over-dehazing since hand-crafted priors are often scenario-specific. Recently, the advent of deep learning has spurred

a shift towards utilizing deep learning for dehazing [4, 7, 13, 25, 33, 48]. These methods typically utilize synthetic paired data for training since real-world hazy and clear image pairs are normally tough to collect. Although improved performance is observed, such paired training paradigm often fails to generalize to real-world scenarios, due to the ill-presenting performance of trained networks that lack real-world information from hazy images. To tackle the bottleneck of paired training, recent studies [24, 40, 43, 47] explore unpaired training for dehazing without the requirements of data pairs. This paradigm enables existing model architectures to be directly trained on real-world data, making it more suitable for real-world image dehazing.

As shown in Figure 1, existing unpaired dehazing methods [9, 40, 43, 47] predominantly leverage Generative Adversarial Networks (GANs) [14] to generate dehazed images. Typically, these methods first produce preliminary dehazed results using a generator, often based on an Encoder-Decoder. They then align the distribution of these results with that of unpaired clear images using a discriminator. However, these methods often struggle to handle images with complex and detailed structures due to limitations in the generator’s ability to model transport mappings. Recent advancements in diffusion models [18, 35, 39] offer an effective alternative. Diffusion models can simulate more intricate transport mappings through an iterative process of adding and removing noise, generating diverse and high-quality dehazed results. Although this capability is difficult for GANs to match, diffusion models must first transform the image into Gaussian noise and then generate the image through a large number of sampling steps. This process imposes limitations on their potential for unpaired dehazing and leads to inferior computational efficiency.

Another key challenge in unpaired dehazing is the way to ensure the structural consistency between hazy and dehazed images, so as to suppress misaligned information caused by unpaired clear images. While CycleGAN [50] serves as a classical solution and has been widely used in previous unpaired dehazing methods [9, 22, 43, 44], it requires additional training of generators and discriminators, leading to additional computational cost. Additionally, we observe that a pre-trained CLIP model [34] can effectively distinguish between hazy and clear images. This insight motivates us to explore improving dehazing by maximizing the distance between hazy textual prompts and dehazed images. However, we find that directly providing textual descriptions is not the optimal solution. This may be due to the fact that the concentration and types of haze in real-world images are extremely complex, and simple textual descriptions fail to capture these characteristics.

To address the aforementioned challenges, we propose a novel framework for real-world image dehazing, namely DehazeSB, consisting of the following contributions:

- We apply Schrödinger Bridge (SB) in our unpaired dehazing framework. Leveraging SB based on optimal transport (OT) theory, we establish direct bridges between hazy and clear image distributions. This enables us to find optimal transport mappings from hazy to clear images, thereby improving dehazing performance. Moreover, SB can generate high-quality images in just a few or even one step, significantly reducing computational overhead.
- To enforce a structure-consistent constraint while minimizing training overhead, we introduce detail-preserving regularization. This ensures content and texture consistency during the dehazing process.
- We propose a novel prompt learning strategy to tailor the textual representations for hazy images. This learned prompt plays a more effective role in representing hazy images instead of direct textual descriptions.
- Extensive quantitative and qualitative experiments show that our method surpasses existing state-of-the-art dehazing methods, including paired or unpaired training.

## 2. Related Work

### 2.1. Image Dehazing

Early prior-based methods focus on obtaining the ASM’s parameters, and then restoring clear images by reserving the ASM. For example, DCP [16] proposes a dark channel prior to estimate the atmospheric light and transmission map. With the development of deep learning, some efforts concentrate on designing networks to estimate the parameters of ASM or directly learn the mapping from hazy to clear images. DehazeNet [4] is the pioneer in estimating transmission maps in an end-to-end manner. C2PNet [48] customizes a curriculum learning to improve dehazing performance. Despite the existence of various proposed networks, their dehazing performance on real-world images remains limited since they are trained on synthetic datasets.

To address the bottleneck of paired training, recent studies have focused on unpaired training strategies to improve the model’s generalization capabilities. For example, RefineDNet [47] integrates the dark channel prior (DCP) into a two-stage dehazing network for unpaired learning. D4+ [44] decomposes the ASM and develops a self-augmented dehazing framework built on CycleGAN [50]. UCL-Dehaze [40] proposes an unpaired contrastive learning paradigm for image dehazing. These methods all employ GANs to generate dehazed images. Despite achieving better performance on real-world hazy images, they still fail to produce satisfactory dehazing results due to the limited transmission mapping capability of the generator.

### 2.2. Schrödinger Bridge based Image Translation

The Schrödinger Bridge [37] problem involves finding the stochastic process that transitions from an initial distribu-

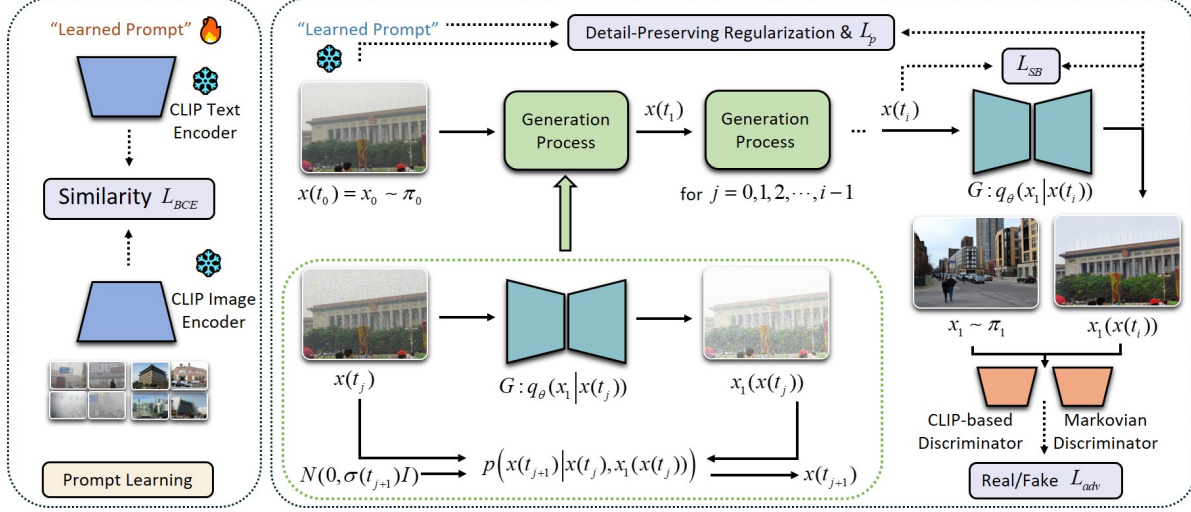


Figure 2. Overview of our method. We first learn a haze-aware prompt using prompt learning. This learned prompt is then used to guide the training of the Schrödinger Bridge (The part within the black dashed box on the right). For SB training, we discretize the unit interval  $[0, 1]$  into  $N$  intervals with uniform spacing, where  $t_j < t_{j+1}$ ,  $t_0 = 0$ , and  $t_N = 1$ .  $x(t_0) = x_0$  denotes the hazy image sampled from  $\pi_0$ .  $x_1$  denotes the unpaired clear image sampled from  $\pi_1$ .  $x_1(x(t_j))$  denotes the generated dehazed image from intermediate states  $x(t_j)$  using generator  $G$ . The generation process involves generating  $x(t_{j+1})$  from  $x(t_j)$  (details are provided within the green dashed box). During the training of the SB, we use the hazy image  $x_0$  to generate an intermediate state  $x(t_i)$  through an iterative generation process with  $j = 0, 1, 2, \dots, i-1$ . Next, we feed  $x(t_i)$  into the generator  $G : q_\theta(x_1 | x(t_i))$  to produce a dehazed image  $x_1(x(t_i))$ . Finally, we calculate the  $L_{adv}$ ,  $L_{SB}$  and  $L_p$  using the unpaired clear image  $x_1$ , the generated dehazed image  $x_1(x(t_i))$ , the hazy image  $x_0$ , and the learned prompt. Furthermore, we impose a detail-preserving regularization between  $x_0$  and  $x_1(x(t_i))$  to enforce structural and detail consistency, ensuring that the dehazed image aligns pixel-by-pixel with the hazy image. In the inference process, we input hazy images directly into generator  $G$  to produce dehazed images with different numbers of function evaluations (NFEs).

tion to a target distribution while adhering to a reference measure. The Schrödinger Bridge provides the flexibility to select arbitrary distributions as both the initial and terminal distributions, making it highly versatile. For instance, I<sup>2</sup>SB [27] proposes the Image-to-Image Schrödinger Bridge, learning nonlinear diffusion processes between two given distributions. UNSB [20] is the first to achieve high-resolution unpaired image translation using adversarial learning. CUNSB-RFIE [8] introduces a context-aware unpaired neural Schrödinger Bridge for retinal fundus image enhancement. However, despite these advancements, applying the Schrödinger Bridge to image dehazing remains challenging, since the degradation mechanisms of images captured under hazy conditions are extremely complex.

### 3. Preliminary

#### 3.1. Schrödinger Bridge

The Schrödinger Bridge problem involves finding an optimal stochastic process  $\{x(t) : t \in [0, 1]\}$  that connects two probability distributions  $\pi_0$  and  $\pi_1$  on  $\mathbb{R}^d$ , while respecting a reference measure  $\mathbb{W}$ , typically chosen to be the Wiener measure. Formally, let  $\Omega$  represent the path space and  $\mathcal{P}(\Omega)$  denote the probability measure on  $\Omega$ . The Schrödinger

Bridge problem can be mathematically formulated as:

$$\mathbb{Q}^{SB} = \arg \min_{\mathbb{Q} \in \mathcal{P}(\Omega)} D_{KL}(\mathbb{Q} \parallel \mathbb{W}) \quad \text{s.t.} \quad \mathbb{Q}_0 = \pi_0, \mathbb{Q}_1 = \pi_1, \quad (2)$$

where  $\mathbb{Q}^{SB}$  denotes the Schrödinger Bridge solution, and  $\mathbb{Q}_t$  corresponds to the marginal distribution of  $\mathbb{Q}$  at time  $t$ .  $D_{KL}(\mathbb{Q} \parallel \mathbb{W})$  represents the Kullback-Leibler divergence. This formulation establishes a probabilistic coupling that enables bidirectional sampling between the distributions. Specifically, given samples  $x_0 \sim \pi_0$ , the bridge  $\mathbb{Q}^{SB}$  facilitates the generation of corresponding samples  $x_1 \sim \pi_1$  through the interpolating process. The reverse direction is equally attainable through time reversal.

#### 3.2. Static Schrödinger Bridge

The Schrödinger Bridge enables the direct learning of optimal transport between arbitrary distributions. However, the inherent temporal dependencies in the full process make the direct optimization of  $\mathbb{Q}^{SB}$  challenging. The Static Schrödinger Bridge (SSB) offers a solution by simplifying the Schrödinger Bridge problem into a more tractable formulation. This reduction establishes an equivalence between the Schrödinger Bridge  $\mathbb{Q}^{SB}$  and its static formulation  $\mathbb{Q}_{01}^{SB}$ , which characterizes the joint distribution of the initial distribution  $\pi_0$  and the terminal distribution  $\pi_1$ .

Let  $\Pi(\pi_0, \pi_1)$  denote the space of joint distributions with marginals  $\pi_0$  and  $\pi_1$ . The SSB problem can be formulated as an entropy-regularized optimal transport problem:

$$\mathbb{Q}_{01}^{\text{SB}} = \arg \min_{\gamma \in \Pi(\pi_0, \pi_1)} \mathbb{E}_{(x_0, x_1) \sim \gamma} [\|x_0 - x_1\|^2] - 2\tau H(\gamma), \quad (3)$$

where  $H(\gamma)$  denotes the entropy, and  $\tau$  controls the amount of randomness in the trajectory. Under this formulation, the marginal distribution  $x(t) : t \in [0, 1]$  can be obtained through conditional Gaussian distributions:

$$p(x(t) | x_0, x_1) \sim \mathcal{N}(x(t); tx_1 + (1-t)x_0, t(1-t)\tau I), \quad (4)$$

where  $I$  is the identity matrix. A crucial self-similarity property emerges in  $\mathbb{Q}_{01}^{\text{SB}}$ , as demonstrated in UNSB [20]. For any sub-interval  $[t_\alpha, t_\beta] \subseteq [0, 1]$ , the restricted process  $Q_{t_\alpha t_\beta}^{\text{SB}}$  remains a Schrödinger Bridge, which can be formulated as conditional Gaussian distributions:

$$\begin{aligned} p(x(t) | x(t_\alpha), x(t_\beta)) &\sim \mathcal{N}(x(t); \mu(t), \sigma(t)), \\ \mu(t) &= s(t)x(t_\beta) + (1-s(t))x(t_\alpha), \\ \sigma(t) &= s(t)(1-s(t))\tau(t_\beta - t_\alpha)I, \end{aligned} \quad (5)$$

where  $s(t) := (t - t_\alpha)/(t_\beta - t_\alpha)$ . This enables recursive interpolation between intermediate states.

## 4. Method

As shown in Figure 2, We propose a novel unpaired dehazing framework, DehazeSB, based on the Schrödinger Bridge. It comprises three components: prompt learning, Schrödinger Bridge, and detail-preserving regularization.

### 4.1. Prompt Learning

Inspired by CLIP’s [26, 30, 34] demonstrated capability for cross-modal alignment, we observe that its discriminative power extends to distinguishing hazy and clear images when provided with textual descriptors (as validated in Figure 3). This insight motivates us to leverage prompts to facilitate dehazing. However, we have empirically observed that generic prompts such as “hazy image” yield sub-optimal results. This limitation arises from the wide variation in haze concentration and distribution found in real-world hazy images, which simplistic prompts fail to adequately capture.

To address this problem, we propose a novel prompt learning that exclusively optimizes haze-aware prompts. Specifically, we randomly initialize a learnable textual prompt  $T_{\text{hazy}}$ . Subsequently, we leverage the pre-trained CLIP’s image encoder  $\Phi_{\text{image}}$  and text encoder  $\Phi_{\text{text}}$  to separately extract features from hazy images  $I_{\text{hazy}}$ , clear images  $I_{\text{clear}}$ , and initialized haze-aware prompt  $T_{\text{hazy}}$ . We train this prompt using a binary cross-entropy (BCE) loss:

$$L_{\text{BCE}} = -(y \log \hat{y} + (1-y) \log(1-\hat{y})), \quad (6)$$

| Prompt              | Left Image Score | Right Image Score |
|---------------------|------------------|-------------------|
| Hazy image.         | 0.93             | 0.88              |
| Rain image.         | 0.63             | 0.81              |
| Low-light image.    | 0.81             | 0.37              |
| Clear image.        | 0.42             | 0.07              |
| Our learned prompt. | 0.97             | 0.95              |

Figure 3. CLIP scores of different prompts. We observe that appropriate prompts are effective in distinguishing between hazy and clear images (for instance, the prompt “hazy image” receives a higher score on hazy images). However, due to the complex degradation characteristics of real-world hazy images, simplistic prompts like “hazy image” fail to accurately capture these nuances. In contrast, our learned haze-aware prompt demonstrates superior effectiveness, achieving the highest scores.

$$\hat{y} = \frac{e^{\cos((\Phi_{\text{image}}(I), \Phi_{\text{text}}(T_{\text{hazy}})))}}{\sum_{i \in \{\text{hazy}, \text{clear}\}} e^{\cos((\Phi_{\text{image}}(I_i), \Phi_{\text{text}}(T_{\text{hazy}})))}}, \quad (7)$$

where  $I \in \{I_{\text{hazy}}, I_{\text{clear}}\}$ , and  $y$  is the label of  $I$ . 0 is for negative sample  $I_{\text{clear}}$  and 1 is for positive sample  $I_{\text{hazy}}$ . The learned haze-aware prompt subsequently guides the training of the Schrödinger Bridge. Specifically, given a generated dehazed image  $I_{\text{dehaze}}$  (denoted by  $x_1(x(t_i))$  in Figure 2) and its hazy counterpart  $I_{\text{hazy}}$  (denoted by  $x_0$ ), we guide the dehazing by pushing the learned haze-aware prompt away from dehazed images. This loss function can also be expressed as Eq. 6, where  $\hat{y}$  is formulated as:

$$\hat{y} = \frac{e^{\cos((\Phi_{\text{image}}(I), \Phi_{\text{text}}(T_{\text{hazy}})))}}{\sum_{i \in \{\text{hazy}, \text{dehaze}\}} e^{\cos((\Phi_{\text{image}}(I_i), \Phi_{\text{text}}(T_{\text{hazy}})))}}, \quad (8)$$

where  $I \in \{I_{\text{hazy}}, I_{\text{dehaze}}\}$ . Specifically, 0 is for negative sample  $I_{\text{dehaze}}$  and 1 is for positive sample  $I_{\text{hazy}}$ .

### 4.2. Schrödinger Bridge

For SB training, we discretize the unit interval  $[0, 1]$  into  $N$  intervals with uniform spacing ( $N = 5$  in our framework). According to the Markov chain decomposition, we can simulate the SB between hazy and clear images as:

$$p(\{x(t_n)\}) = p(x(t_N)|x(t_{N-1})) \cdots p(x(t_1)|x(t_0))p(x(t_0)), \quad (9)$$

where  $t_i < t_{i+1}$ ,  $t_0 = 0$ , and  $t_N = 1$ .  $\{x(t_n)\}$  represents a partition  $\{x(t_i)\}_{i=0}^N$  of the unit interval  $[0, 1]$ . Given the initial hazy image distribution  $p(x(t_0))$ , learning the transition probabilities  $p(x(t_{i+1})|x(t_i))$  enables recursive



sampling to approximate the target distribution  $p(x(t_N))$ , where  $p(x(t_0))$  and  $p(x(t_N))$  are also referred to as  $p(x_0)$  and  $p(x_1)$ . Therefore, we need to design a network with parameters  $\theta_i$  as the generator  $G : q_{\theta_i}(x(t_{i+1}) | x(t_i))$  to modulate  $p(x(t_{i+1}) | x(t_i))$ , allowing us to sample from the initial distribution and obtain the target distribution.

However, it is impractical to devise a separate generator  $G$  for each time step. Following the UNSB [20], we devise an elaborated generator  $G : q_{\theta}(x(t_N) | x(t_i))$  conditioned on time step  $t_i$ , which can also be denoted as  $G : q_{\theta}(x_1 | x(t_i))$ . This generator directly predicts the target  $x_1$  from any intermediate state  $x(t_i)$ . In doing so, the optimization objective can be expressed as:

$$\begin{aligned} L_{SB} &:= \mathbb{E}_{q_{\theta}(x(t_i), x_1)} [\|x(t_i) - x_1\|^2] \\ &\quad - 2\tau(1 - t_i)H(q_{\theta}(x(t_i), x_1)) \\ \text{s.t. } L_{adv} &:= D_{KL}(q_{\theta}(x_1) \| p(x_1)) = 0. \end{aligned} \quad (10)$$

Using Lagrange multipliers, we can transform the optimization objective into a loss function:

$$L := L_{adv} + \lambda_{SB} L_{SB}. \quad (11)$$

The training pipeline is illustrated in Figure 2. Starting from an initial sample  $x(t_0) = x_0 \sim \pi_0$ , we progressively generate intermediate states  $\{x(t_j)\}_{j=1}^i$  through a Markov chain process. After obtaining  $x(t_i)$ , we use the generator  $G : q_{\theta}(x_1 | x(t_i))$  to produce the dehazed image  $x_1(x(t_i))$ . We then calculate the  $L_{SB}$  and  $L_{adv}$  in Eq. 10 using the pairs  $(x(t_i), x_1(x(t_i)))$  and  $(x_1(x(t_i)), x_1)$ . Note that we randomly choose different time steps  $t_i$  to optimize during the training, thus our model can generate target images with an arbitrary number of function evaluations (NFEs). For the generation process of  $x(t_{j+1})$  at each step  $j = 0, 1, 2, \dots, i-1$ , we first predict the target domain sample  $x_1(x(t_j))$  using the generator  $G : q_{\theta}(x_1 | x(t_j))$ . Subsequently we generate  $x(t_{j+1})$  through the Eq. 5, which can be expressed as:

$$\begin{aligned} p(x(t_{j+1}) | x(t_j), x_1(x(t_j))) &\sim \\ \mathcal{N}(x(t_{j+1}); \mu(t_{j+1}), \sigma(t_{j+1})), \\ \mu(t_{j+1}) &= s(t_{j+1})x_1(x(t_j)) + (1 - s(t_{j+1}))x(t_j), \\ \sigma(t_{j+1}) &= s(t_{j+1})(1 - s(t_{j+1}))\tau(1 - t_j)I. \end{aligned} \quad (12)$$

To align the distribution of generated images  $q_{\theta}(x_1)$  with the target distribution  $p(x_1)$ , we replace the KL divergence in Eq. 10 with a dual-discriminator adversarial strategy. Specifically, We first employ a Markovian discriminator which distinguishes samples on the patch level since it is effective at capturing details and textures in local characteristics. To complement patch-level analysis, we introduce a CLIP-based discriminator [21] that assesses overall structural coherence and scene consistency. This mitigates limitations of purely local evaluation, which can

overlook implausible global arrangements. By combining these discriminators, our method simultaneously enhances local realism and global plausibility. Finally, We compute  $H(q_{\theta}(x(t_i), x_1))$  in a manner similar to the approach used in UNSB [20], as detailed in our supplementary materials.

### 4.3. Detail-Preserving Regularization

Another critical challenge in unpaired image dehazing is detail preservation. The generated images must not only display high visual quality but also maintain fidelity in details and textures compared to the original images. Although CycleGAN [50] is a classic solution for this problem, it necessitates the training of additional generators and discriminators, leading to high computational demands. To overcome this limitation, we introduce a detail-preserving regularization that includes PatchNCE regularization, physical prior regularization, and high-frequency detail regularization.

#### 4.3.1. PatchNCE Regularization

Following the CUT [32], we employ PatchNCE regularization to enhance the generator’s ability to preserve content consistency during image dehazing. Specifically, PatchNCE regularization leverages contrastive learning to enforce similarity between corresponding patches in the input and output. This helps the generator learn to maintain important structural details and textures, thereby improving the overall quality of the dehazed images. For more detailed information, please refer to our supplementary materials.

#### 4.3.2. Physical Prior Regularization

Previous studies [5, 43, 47] have demonstrated that using physical priors can enhance real-world image dehazing. Moreover, they enable us to preserve as much detail as possible. Specifically, we process the hazy image  $I$  (also referred to as  $x_0$ ) using Dark Channel Prior (DCP) [16], obtaining the atmospheric light  $A$ , coarse transmission map  $t$ , and dehazed image  $J_{dcp}$ . We then feed  $t$  into a UNet [36] to obtain a refined transmission map  $t_{ref}$ . Finally, we reconstruct the hazy image  $I_{phy}$  according to the Eq. 1 and formulate the physical prior regularization as follows:

$$L_{phy} = L_{rec}(I, I_{phy}), \quad (13)$$

where  $I_{phy} = Jt_{ref} + A(1 - t_{ref})$  refers to the reconstructed hazy image derived using the ASM, and  $J$  denotes the generated dehazed image  $x_1(x(t_i))$ .  $L_{rec}$  is the combined distance of  $L_1$  and LPIPS. [46].

#### 4.3.3. High-Frequency Detail Regularization

To enhance structural fidelity in the restored images while preserving high-frequency details, we introduce a high-frequency detail regularization that includes Discrete Fourier Transform (DFT) loss, Structural Similarity Index Measure (SSIM) loss, and Sobel Gradient loss. We provide more detailed information in our supplementary materials.



Figure 4. Visual comparison of samples from RTTS and Haze2020. Our method can effectively remove haze and generate high-quality images with natural color and realistic contrast. **More than 40 visual results are presented in our supplementary materials.**

|             |                  | RTTS          |              |               |              | Haze2020      |              |               |              |
|-------------|------------------|---------------|--------------|---------------|--------------|---------------|--------------|---------------|--------------|
| Type        | Method           | FID↓          | NIQE↓        | MUSIQ↑        | MANIQA ↑     | FID↓          | NIQE↓        | MUSIQ↑        | MANIQA↑      |
| Prior-based | DCP [16]         | 73.017        | 4.271        | 52.935        | 0.119        | 91.948        | 3.827        | 54.375        | 0.121        |
| Paired      | MBFormer [33]    | 66.023        | 4.874        | 53.576        | 0.139        | 82.596        | 4.128        | 55.550        | <u>0.141</u> |
| Paired      | C2PNet [48]      | 66.117        | 5.037        | 53.960        | 0.142        | 83.959        | 4.206        | 54.565        | 0.138        |
| Paired      | KANet [13]       | 64.963        | 4.339        | 54.513        | 0.110        | 84.888        | <b>3.742</b> | 56.411        | 0.127        |
| Paired      | DEANet [6]       | 66.355        | 4.805        | 53.628        | 0.132        | 84.197        | 3.976        | 54.757        | 0.135        |
| Paired      | Diff-Plugin [28] | 65.787        | 5.334        | 50.740        | 0.095        | 80.965        | 4.407        | 52.752        | 0.111        |
| Paired      | OneRestore [15]  | 65.934        | 5.321        | 51.380        | 0.114        | 84.276        | 4.365        | 52.066        | 0.116        |
| Paired      | SGDN [10]        | 78.018        | 5.716        | 44.858        | 0.081        | 89.061        | 5.914        | 46.326        | 0.094        |
| Unpaired    | CUT [32]         | 98.771        | 3.938        | <u>59.798</u> | <u>0.146</u> | 75.625        | 4.261        | <u>58.668</u> | 0.135        |
| Unpaired    | UNSB [8]         | <u>56.668</u> | <u>3.834</u> | 55.048        | 0.132        | <u>72.812</u> | 4.137        | 55.384        | 0.132        |
| Unpaired    | YOLY [24]        | 69.996        | 4.553        | 51.874        | 0.129        | 85.648        | 3.937        | 54.164        | 0.138        |
| Unpaired    | RefineDNet [47]  | 65.076        | 4.012        | 56.117        | 0.108        | 88.229        | 3.972        | 54.779        | 0.122        |
| Unpaired    | D4 [43]          | 69.400        | 4.637        | 58.445        | 0.139        | 87.536        | 3.971        | 53.458        | 0.119        |
| Unpaired    | D4+ [44]         | 67.687        | 4.274        | 53.599        | 0.131        | 87.101        | 3.865        | 53.612        | 0.124        |
| Unpaired    | Ours             | <b>53.120</b> | <b>3.760</b> | <b>60.114</b> | <b>0.153</b> | <b>69.796</b> | <u>3.743</u> | <b>59.256</b> | <b>0.150</b> |

Table 1. Quantitative results on RTTS and Haze2020. The best results are denoted in **bold**, and the second-best results are underlined.

The final loss function can be formulated as:

$$L = L_{adv} + \lambda_{SB}L_{SB} + \lambda_pL_p + \lambda_{NCE}L_{NCE} + \lambda_{phy}L_{phy} + \lambda_{hfd}L_{hfd}, \quad (14)$$

where  $L_{NCE}$ ,  $L_{phy}$ , and  $L_{hfd}$  denote the PatchNCE, physical prior, and high-frequency detail regularization loss. Each term is weighted by its corresponding coefficients  $\lambda$ : 1, 1, 1, 0.5, and 0.5 respectively.

## 5. Experiments and Discussion

Our method enables direct training on unpaired real-world hazy and clear images. Specifically, we collect over 7,000 real hazy images from the RESIDE [23] for our training set

of hazy images. Additionally, we gather over 10,000 clear images from the SOTS (a subset of RESIDE) and ADE20K [49] to serve as our training set of clear images. To comprehensively evaluate our method, we conduct extensive quantitative and qualitative comparisons using multiple real-world datasets: RTTS, URHI, Haze2020, OHAZE, IHAZE, and Fattal’s dataset. Among them, RTTS and URHI are subsets of RESIDE, each containing over 4,000 hazy images. Haze2020, introduced by DA [38], includes more than 1,000 real-world images. OHAZE [2] and IHAZE [1] contain 45 and 55 pairs of hazy images, respectively, generated using a haze machine. Fattal’s dataset [12] comprises over 30 real-world hazy images. More training details and parameters are in the supplementary materials.

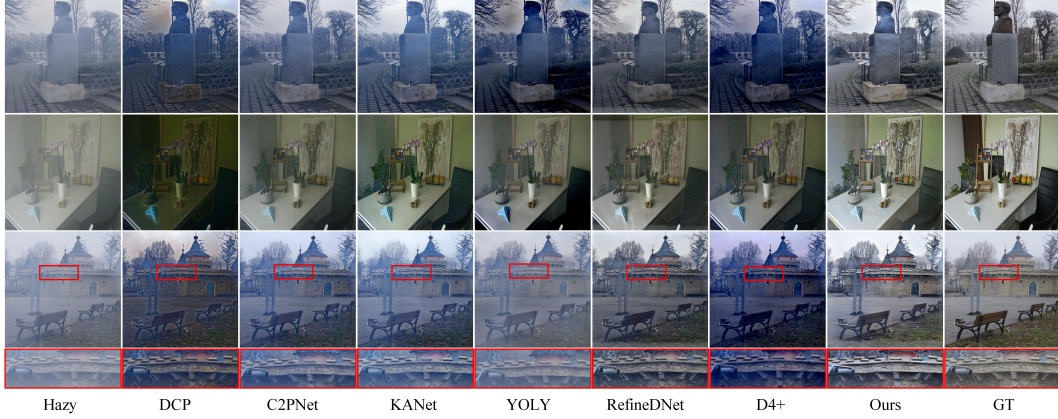


Figure 5. Visual comparison of samples from OHAZE and IHAZE.

| Method      | PSNR $\uparrow$ | SSIM $\uparrow$ | LPIPS $\downarrow$ | VSI $\uparrow$ |
|-------------|-----------------|-----------------|--------------------|----------------|
| DCP         | 17.005          | 0.819           | 0.242              | 0.945          |
| MBFormer    | 15.243          | 0.672           | 0.339              | 0.911          |
| C2PNet      | 18.014          | 0.708           | 0.317              | 0.929          |
| KANet       | 17.713          | 0.814           | 0.265              | 0.939          |
| DEANet      | 14.687          | 0.691           | 0.440              | 0.880          |
| Diff-Plugin | 16.470          | 0.526           | 0.364              | 0.920          |
| OneRestore  | 17.458          | 0.740           | 0.282              | 0.924          |
| SGDN        | 18.163          | 0.682           | 0.381              | 0.953          |
| CUT         | 15.927          | 0.713           | 0.341              | 0.936          |
| UNSB        | 15.018          | 0.648           | 0.392              | 0.940          |
| YOLY        | 14.974          | 0.406           | 0.425              | 0.914          |
| RefineDNet  | 18.693          | 0.755           | 0.260              | 0.954          |
| D4          | 16.767          | 0.690           | 0.290              | 0.939          |
| D4+         | 17.336          | 0.677           | 0.301              | 0.947          |
| Ours        | <b>18.829</b>   | <b>0.838</b>    | <b>0.223</b>       | <b>0.961</b>   |

Table 2. Quantitative results on OHAZE.

We compare our method against several state-of-the-art methods. Among them, DCP is a prior-based dehazing method. CUT and UNSB are originally proposed for unpaired image translation. For images with available ground truth (GT), we evaluate them using full-reference metrics such as PSNR, SSIM [41], LPIPS, and VSI [45]. For images without GT, we use no-reference metrics, including FID [17], NIQE [29], MUSIQ [19], and MANIQA [42].

### 5.1. Results on RTTS and Haze2020

We conduct qualitative comparisons on RTTS and Haze2020, and zoom in on local details within partial images. As shown in Figure 4, DCP effectively processes images but tends to over-enhance results due to the limitations of hand-crafted priors. C2PNet struggles with images because it is trained on synthetic datasets, which have a domain gap with real-world data. KANet shows promis-

ing performance by employing an advanced data synthesis strategy. However, KANet still falls short of fully removing haze due to the inherent limitations of paired training. Unpaired dehazing methods like YOLY, RefineDNet, and D4+ can dehaze images to some extent. However, these methods often produce sub-optimal results due to the limited transport mapping capabilities of GAN generators, resulting in artifacts and insufficient detail. In contrast, our proposed method leverages the Schrödinger Bridge to directly learn optimal transport mappings in an unpaired training framework. This approach generates more realistic and natural images with rich details, textures, and high contrast.

Table 1 presents a quantitative comparison of Haze2020 and RTTS. Our method achieves the best quantitative results on RTTS and excels in several metrics on Haze2020. For NIQE, our approach ranks second, slightly behind KANet. This discrepancy likely results from the introduction of physical prior regularization in our method. We introduce physical prior regularization to ensure our method effectively removes haze while preserving the original image’s fine details and textures. Although this regularization slightly compromised NIQE scores, we believe the overall improvement in image quality justifies this trade-off.

### 5.2. Results on OHAZE and IHAZE

Figure 5 and Table 2 present results on OHAZE and IHAZE. Notably, we do not retrain our model on these datasets but directly evaluate them to demonstrate the generalization capability of our method. The experimental results indicate that our method outperforms other approaches, achieving superior metrics while also producing visually pleasing dehazed images. The results for URHI and Fattal’s dataset are provided in the supplementary materials.

### 5.3. Ablation Study

We conduct a series of ablation studies on Haze2020 and OHAZE to validate the effectiveness of each component,





Figure 6. Ablation study of each component. (a) Hazy image. (b) Backbone. (c) Backbone + PL. (d) Backbone + DPR. (e) Ours.

|          |        |              |              |               |
|----------|--------|--------------|--------------|---------------|
| Backbone | ✓      | ✓            | ✓            | ✓             |
| PL       |        | ✓            |              | ✓             |
| DPR      |        |              | ✓            | ✓             |
| FID ↓    | 80.260 | 73.968       | 75.192       | <b>69.796</b> |
| NIQE ↓   | 3.712  | <b>3.690</b> | 3.981        | 3.743         |
| MUSIQ ↑  | 54.414 | 59.109       | 56.550       | <b>59.256</b> |
| MANIQA ↑ | 0.105  | 0.144        | 0.133        | <b>0.150</b>  |
| PSNR ↑   | 17.410 | 17.445       | 18.687       | <b>18.829</b> |
| SSIM ↑   | 0.777  | 0.796        | <b>0.839</b> | 0.838         |
| LPIPS ↓  | 0.282  | 0.298        | 0.253        | <b>0.223</b>  |
| VSI ↑    | 0.939  | 0.937        | 0.952        | <b>0.961</b>  |

Table 3. Ablation study of each component.

including the Schrödinger Bridge (SB), Prompt Learning (PL), and Detail-Preserving Regularization (DPR). Note that our method employs unpaired training, which does not utilize ground truth (GT). Therefore, PatchNCE regularization is essential to prevent gradient explosion. In the following ablation study, our backbone includes PatchNCE regularization by default. We construct the following variants: **Backbone**: Removing both PL and DPR. **Backbone + PL**: Removing DPR. **Backbone + DPR**: Removing PL. **Ours**: Our method. As shown in Table 3 and Figure 6, our proposed method achieves the best performance in both visual appeal and most metrics, striking an effective balance between perceptual quality and distortion. This validates that each component plays a critical role in improving dehazing performance.

### 5.3.1. Ablation of Schrödinger Bridge

We perform an ablation study to evaluate how discriminators affect the results within our framework. As illustrated in Figure 7, by employing both a Markovian Discriminator (MD) and a CLIP-based Discriminator (CD), we can simultaneously preserve the local details and ensure the global quality of the dehazed images, resulting in high-quality results. Moreover, the MD plays a crucial role in our method due to our use of PatchNCE regularization, which minimizes the distance between a patch in the dehazed image and its corresponding patch in the hazy image at the same location. Without the MD to evaluate images at the patch level, the method will fail to effectively remove haze.

Additionally, we investigate the impact of the number of intervals used in our method, with detailed information



Figure 7. Ablation study of discriminators. (a) Hazy image. (b) Remove MD. (c) Remove CD. (d) Ours.

|          |        |        |              |               |
|----------|--------|--------|--------------|---------------|
| Backbone | ✓      | ✓      | ✓            | ✓             |
| PPR      |        | ✓      |              | ✓             |
| HFDR     |        |        | ✓            | ✓             |
| FID ↓    | 73.968 | 74.372 | 73.727       | <b>69.796</b> |
| NIQE ↓   | 3.690  | 3.753  | <b>3.655</b> | 3.743         |
| MUSIQ ↑  | 59.109 | 55.770 | 58.526       | <b>59.256</b> |
| MANIQA ↑ | 0.144  | 0.143  | 0.142        | <b>0.150</b>  |
| PSNR ↑   | 17.445 | 18.085 | 17.534       | <b>18.829</b> |
| SSIM ↑   | 0.796  | 0.812  | 0.805        | <b>0.838</b>  |
| LPIPS ↓  | 0.298  | 0.290  | 0.267        | <b>0.223</b>  |
| VSI ↑    | 0.937  | 0.940  | 0.940        | <b>0.961</b>  |

Table 4. Ablation study of detail-preservation regularization.

provided in the supplementary materials.

### 5.3.2. Ablation of detail-preservation regularization

We validate the effectiveness of detail-preservation regularization, which includes physical prior regularization (PPR) and high-frequency detail regularization (HFDR). Table 4 demonstrates that both types of regularization contribute to improved performance. We also analyze the impact of varying weights of them in our supplementary materials.

## 6. Conclusion and Discussion

In this paper, we apply the Schrödinger Bridge in real-world image dehazing with unpaired training, named DehazeSB. By learning the optimal transport mappings from hazy to clear image distributions and enforcing detail-preserving regularization, we achieve high-quality dehazing. Furthermore, inspired by the observation that pre-trained CLIP models can accurately distinguish between hazy and clear images, we introduce a novel prompt learning to enhance dehazing. Extensive experiments demonstrate its effectiveness in producing high-quality dehazed results.

While our Schrödinger Bridge-based approach shows significant superiority in unpaired image dehazing, it has some limitations. First, it depends on a learned haze-aware prompt, making it sensitive to the quality and diversity of the training data. If the training set lacks variability in haze conditions, the model’s generalization may suffer. Second, although our detail-preserving improves fidelity in textures and structures, it struggles with highly complex or fine-grained details, especially in images with dense haze.



## References

- [1] Cosmin Ancuti, Codruta O Ancuti, Radu Timofte, and Christophe De Vleeschouwer. I-haze: A dehazing benchmark with real hazy and haze-free indoor images. In *Advanced Concepts for Intelligent Vision Systems: 19th International Conference, ACIVS 2018, Poitiers, France, September 24–27, 2018, Proceedings 19*, pages 620–631. Springer, 2018. 6
- [2] Codruta O Ancuti, Cosmin Ancuti, Radu Timofte, and Christophe De Vleeschouwer. O-haze: a dehazing benchmark with real hazy and haze-free outdoor images. In *Proceedings of the IEEE conference on computer vision and pattern recognition workshops*, pages 754–762, 2018. 6
- [3] Dana Berman, Shai Avidan, et al. Non-local image dehazing. In *Proceedings of the IEEE conference on computer vision and pattern recognition*, pages 1674–1682, 2016. 1
- [4] Bolun Cai, Xiangmin Xu, Kui Jia, Chunmei Qing, and Dacheng Tao. Dehazenet: An end-to-end system for single image haze removal. *IEEE transactions on image processing*, 25(11):5187–5198, 2016. 2
- [5] Zeyuan Chen, Yangchao Wang, Yang Yang, and Dong Liu. Psd: Principled synthetic-to-real dehazing guided by physical priors. In *Proceedings of the IEEE/CVF conference on computer vision and pattern recognition*, pages 7180–7189, 2021. 5
- [6] Zixuan Chen, Zewei He, and Zhe-Ming Lu. Dea-net: Single image dehazing based on detail-enhanced convolution and content-guided attention. *IEEE Transactions on Image Processing*, 2024. 6
- [7] Hang Dong, Jinshan Pan, Lei Xiang, Zhe Hu, Xinyi Zhang, Fei Wang, and Ming-Hsuan Yang. Multi-scale boosted dehazing network with dense feature fusion. In *Proceedings of the IEEE/CVF conference on computer vision and pattern recognition*, pages 2157–2167, 2020. 2
- [8] Xuanzhao Dong, Vamsi Krishna Vasa, Wenhui Zhu, Peijie Qiu, Xiwen Chen, Yi Su, Yujian Xiong, Zhangsihao Yang, Yanxi Chen, and Yalin Wang. Cunsb-rfie: Context-aware unpaired neural schrodinger bridge in retinal fundus image enhancement. In *Proceedings of the Winter Conference on Applications of Computer Vision (WACV)*, pages 4502–4511, 2025. 3, 6
- [9] Deniz Engin, Anil Genç, and Hazim Kemal Ekenel. Cycle-dehaze: Enhanced cyclegan for single image dehazing. In *Proceedings of the IEEE conference on computer vision and pattern recognition workshops*, pages 825–833, 2018. 2
- [10] Wenxuan Fang, Junkai Fan, Yu Zheng, Jiangwei Weng, Ying Tai, and Jun Li. Guided real image dehazing using ycbcr color space. In *Proceedings of the AAAI Conference on Artificial Intelligence*, pages 2906–2914, 2025. 6
- [11] Ali Farhadi and Joseph Redmon. Yolov3: An incremental improvement. In *Computer vision and pattern recognition*, pages 1–6. Springer Berlin/Heidelberg, Germany, 2018. 1
- [12] Raanan Fattal. Dehazing using color-lines. *ACM transactions on graphics (TOG)*, 34(1):1–14, 2014. 6
- [13] Yuxin Feng, Long Ma, Xiaozhe Meng, Fan Zhou, Risheng Liu, and Zhuo Su. Advancing real-world image dehazing: perspective, modules, and training. *IEEE Transactions on Pattern Analysis and Machine Intelligence*, 2024. 2, 6
- [14] Ian Goodfellow, Jean Pouget-Abadie, Mehdi Mirza, Bing Xu, David Warde-Farley, Sherjil Ozair, Aaron Courville, and Yoshua Bengio. Generative adversarial networks. *Communications of the ACM*, 63(11):139–144, 2020. 2
- [15] Yu Guo, Yuan Gao, Yuxu Lu, Huilin Zhu, Ryan Wen Liu, and Shengfeng He. Onerestore: A universal restoration framework for composite degradation. In *European Conference on Computer Vision*, pages 255–272. Springer, 2024. 6
- [16] Kaiming He, Jian Sun, and Xiaoou Tang. Single image haze removal using dark channel prior. *IEEE transactions on pattern analysis and machine intelligence*, 33(12):2341–2353, 2010. 1, 2, 5, 6
- [17] Martin Heusel, Hubert Ramsauer, Thomas Unterthiner, Bernhard Nessler, and Sepp Hochreiter. Gans trained by a two time-scale update rule converge to a local nash equilibrium. *Advances in neural information processing systems*, 30, 2017. 7
- [18] Jonathan Ho, Ajay Jain, and Pieter Abbeel. Denoising diffusion probabilistic models. *Advances in neural information processing systems*, 33:6840–6851, 2020. 2
- [19] Junjie Ke, Qifei Wang, Yilin Wang, Peyman Milanfar, and Feng Yang. Musiq: Multi-scale image quality transformer. In *Proceedings of the IEEE/CVF international conference on computer vision*, pages 5148–5157, 2021. 7
- [20] Beomsu Kim, Gihyun Kwon, Kwanyoung Kim, and Jong Chul Ye. Unpaired image-to-image translation via neural schrödinger bridge. In *The Twelfth International Conference on Learning Representations*, 2024. 3, 4, 5
- [21] Nupur Kumari, Richard Zhang, Eli Shechtman, and Jun-Yan Zhu. Ensembling off-the-shelf models for gan training. In *Proceedings of the IEEE/CVF conference on computer vision and pattern recognition*, pages 10651–10662, 2022. 5
- [22] Yunwei Lan, Zhigao Cui, Chang Liu, Jialun Peng, Nian Wang, Xin Luo, and Dong Liu. Exploiting diffusion prior for real-world image dehazing with unpaired training. In *Proceedings of the AAAI Conference on Artificial Intelligence*, pages 4455–4463, 2025. 2
- [23] Boyi Li, Wenqi Ren, Dengpan Fu, Dacheng Tao, Dan Feng, Wenjun Zeng, and Zhangyang Wang. Benchmarking single-image dehazing and beyond. *IEEE Transactions on Image Processing*, 28(1):492–505, 2018. 6
- [24] Boyun Li, Yuanbiao Gou, Shuhang Gu, Jerry Zitao Liu, Joey Tianyi Zhou, and Xi Peng. You only look yourself: Unsupervised and untrained single image dehazing neural network. *International Journal of Computer Vision*, 129:1754–1767, 2021. 2, 6
- [25] Zhuoyuan Li, Junqi Liao, Chuanbo Tang, Haotian Zhang, Yuqi Li, Yifan Bian, Xihua Sheng, Xinmin Feng, Yao Li, Changsheng Gao, et al. Ustc-td: A test dataset and benchmark for image and video coding in 2020s. *arXiv preprint arXiv:2409.08481*, 2024. 2
- [26] Zhixin Liang, Chongyi Li, Shangchen Zhou, Ruicheng Feng, and Chen Change Loy. Iterative prompt learning for unsupervised backlit image enhancement. In *Proceedings of the IEEE/CVF International Conference on Computer Vision*, pages 8094–8103, 2023. 4

- [27] Guan-Hong Liu, Arash Vahdat, De-An Huang, Evangelos A. Theodorou, Weili Nie, and Anima Anandkumar. I<sup>2</sup>sb: Image-to-image schrödinger bridge. In *Proceedings of the 40th International Conference on Machine Learning*. JMLR.org, 2023. 3
- [28] Yuhao Liu, Zhanghan Ke, Fang Liu, Nanxuan Zhao, and Rynson WH Lau. Diff-plugin: Revitalizing details for diffusion-based low-level tasks. In *Proceedings of the IEEE/CVF Conference on Computer Vision and Pattern Recognition*, pages 4197–4208, 2024. 6
- [29] Anish Mittal, Rajiv Soundararajan, and Alan C Bovik. Making a “completely blind” image quality analyzer. *IEEE Signal processing letters*, 20(3):209–212, 2012. 7
- [30] Igor Morawski, Kai He, Shusil Dangi, and Winston H Hsu. Unsupervised image prior via prompt learning and clip semantic guidance for low-light image enhancement. In *Proceedings of the IEEE/CVF Conference on Computer Vision and Pattern Recognition*, pages 5971–5981, 2024. 4
- [31] Shree K Nayar and Srinivasa G Narasimhan. Vision in bad weather. In *Proceedings of the seventh IEEE international conference on computer vision*, pages 820–827. IEEE, 1999. 1
- [32] Taesung Park, Alexei A Efros, Richard Zhang, and Jun-Yan Zhu. Contrastive learning for unpaired image-to-image translation. In *Computer Vision—ECCV 2020: 16th European Conference, Glasgow, UK, August 23–28, 2020, Proceedings, Part IX 16*, pages 319–345. Springer, 2020. 5, 6
- [33] Yuwei Qiu, Kaihao Zhang, Chenxi Wang, Wenhan Luo, Hongdong Li, and Zhi Jin. Mb-taylorformer: Multi-branch efficient transformer expanded by taylor formula for image dehazing. In *Proceedings of the IEEE/CVF International Conference on Computer Vision*, pages 12802–12813, 2023. 2, 6
- [34] Alec Radford, Jong Wook Kim, Chris Hallacy, Aditya Ramesh, Gabriel Goh, Sandhini Agarwal, Girish Sastry, Amanda Askell, Pamela Mishkin, Jack Clark, Gretchen Krueger, and Ilya Sutskever. Learning Transferable Visual Models From Natural Language Supervision. In *ICML*, pages 8748–8763, 2021. 2, 4
- [35] Robin Rombach, Andreas Blattmann, Dominik Lorenz, Patrick Esser, and Björn Ommer. High-resolution image synthesis with latent diffusion models. In *Proceedings of the IEEE/CVF conference on computer vision and pattern recognition*, pages 10684–10695, 2022. 2
- [36] Olaf Ronneberger, Philipp Fischer, and Thomas Brox. U-net: Convolutional networks for biomedical image segmentation. In *Medical image computing and computer-assisted intervention—MICCAI 2015: 18th international conference, Munich, Germany, October 5–9, 2015, proceedings, part III 18*, pages 234–241. Springer, 2015. 5
- [37] Erwin Schrödinger. Sur la théorie relativiste de l’électron et l’interprétation de la mécanique quantique. In *Annales de l’institut Henri Poincaré*, pages 269–310, 1932. 2
- [38] Yuanjie Shao, Lerenhan Li, Wenqi Ren, Changxin Gao, and Nong Sang. Domain adaptation for image dehazing. In *Proceedings of the IEEE/CVF conference on computer vision and pattern recognition*, pages 2808–2817, 2020. 6
- [39] Jiaming Song, Chenlin Meng, and Stefano Ermon. Denoising diffusion implicit models. In *International Conference on Learning Representations*, 2021. 2
- [40] Yongzhen Wang, Xuefeng Yan, Fu Lee Wang, Haoran Xie, Wenhan Yang, Xiao-Ping Zhang, Jing Qin, and Mingqiang Wei. Ucl-dehaze: Towards real-world image dehazing via unsupervised contrastive learning. *IEEE Transactions on Image Processing*, 2024. 2
- [41] Zhou Wang, Alan C Bovik, Hamid R Sheikh, and Eero P Simoncelli. Image quality assessment: from error visibility to structural similarity. *IEEE transactions on image processing*, 13(4):600–612, 2004. 7
- [42] Sidi Yang, Tianhe Wu, Shuwei Shi, Shanshan Lao, Yuan Gong, Mingdeng Cao, Jiahao Wang, and Yujiu Yang. Maniqa: Multi-dimension attention network for no-reference image quality assessment. In *Proceedings of the IEEE/CVF conference on computer vision and pattern recognition*, pages 1191–1200, 2022. 7
- [43] Yang Yang, Chaoyue Wang, Risheng Liu, Lin Zhang, Xiaojie Guo, and Dacheng Tao. Self-augmented unpaired image dehazing via density and depth decomposition. In *Proceedings of the IEEE/CVF conference on computer vision and pattern recognition*, pages 2037–2046, 2022. 2, 5, 6
- [44] Yang Yang, Chaoyue Wang, Xiaojie Guo, and Dacheng Tao. Robust unpaired image dehazing via density and depth decomposition. *International Journal of Computer Vision*, 132(5):1557–1577, 2024. 2, 6
- [45] Lin Zhang, Ying Shen, and Hongyu Li. Vsi: A visual saliency-induced index for perceptual image quality assessment. *IEEE Transactions on Image processing*, 23(10):4270–4281, 2014. 7
- [46] Richard Zhang, Phillip Isola, Alexei A Efros, Eli Shechtman, and Oliver Wang. The unreasonable effectiveness of deep features as a perceptual metric. In *Proceedings of the IEEE conference on computer vision and pattern recognition*, pages 586–595, 2018. 5
- [47] Shiyu Zhao, Lin Zhang, Ying Shen, and Yicong Zhou. Refinednet: A weakly supervised refinement framework for single image dehazing. *IEEE Transactions on Image Processing*, 30:3391–3404, 2021. 2, 5, 6
- [48] Yu Zheng, Jiahui Zhan, Shengfeng He, Junyu Dong, and Yong Du. Curricular contrastive regularization for physics-aware single image dehazing. In *Proceedings of the IEEE/CVF conference on computer vision and pattern recognition*, pages 5785–5794, 2023. 2, 6
- [49] Bolei Zhou, Hang Zhao, Xavier Puig, Tete Xiao, Sanja Fidler, Adela Barriuso, and Antonio Torralba. Semantic understanding of scenes through the ade20k dataset. *International Journal of Computer Vision*, 127:302–321, 2019. 6
- [50] Jun-Yan Zhu, Taesung Park, Phillip Isola, and Alexei A Efros. Unpaired image-to-image translation using cycle-consistent adversarial networks. In *Proceedings of the IEEE international conference on computer vision*, pages 2223–2232, 2017. 2, 5
- [51] Qingsong Zhu, Jiaming Mai, and Ling Shao. A fast single image haze removal algorithm using color attenuation prior. *IEEE transactions on image processing*, 24(11):3522–3533, 2015. 1